Materials Physics and Mechanics 46 (2020) 88-98 Received: September 25, 2020

STUDY OF THE DEFORMATION AND FRACTURE OF ZIRCONIUM ALLOYS UNDER DYNAMIC LOADING

A.I. Romanov[1], V.A. Panov[1], M.A. Samsonov[1], D.E. Chirkin[1], A.M. Bragov[2*], L.A. Igumnov[2], A.Yu. Konstantinov[2], A.K. Lomunov[2]

[1]Joint Stock Company "Afrikantov OKB Mechanical Engineering", Burnakovsky proezd, 15, Nizhny Novgorod, 603074, Russia

[2]Lobachevsky State University of Nizhny Novgorod, 23 Prospekt Gagarina (Gagarin Avenue) BLDG 6, Nizhny Novgorod, 603950, Russia

*e-mail: bragov@mech.unn.ru

Abstract. The main objective of the present work is the experimental and theoretical investigation of the mechanical properties of the zirconium alloys E110 and E635 in a wide range of strain rates ($10^{-4}\div3\cdot10^{3}$ c^{-1}) and at different temperatures (20°C÷350°C). The strain rate and temperature dependencies of deformation diagrams and strength characteristics under tension and compression have been received using the experimental study. The investigated materials have shown sensitivity to strain rate and temperature. Experimental data have been used to identify some LS-DYNA's material models.

Keywords: experimental investigation, strain rate, model, nuclear energy, dynamics, temperature, flow stress, plastic strain, ultimate strain

1. Introduction

The nuclear industry and energy have special requirements for the materials used. Conventional steels do not pass on safety indicators. Special alloys based on zirconium (Zr) have been developed for this industry. Zirconium is one of the key structural metals in nuclear energy; it is the main component of the alloys used to make the shell of the fuel elements of nuclear reactors. Zirconium alloys have a fairly high corrosion resistance with respect to water and steam and a relatively small cross-section for absorption of thermal neutrons. These alloys favorably differ from pure zirconium in the best mechanical properties. For example, alloy E110 is used as a structural material for the components of the fuel assembly. Currently, this material is the main material for the casings of the fuel rods, spacing grids, and in some cases the guide channels, for PWR (Pressurized water reactor) type reactors. Preservation of high ductility by E110 alloy in combination with corrosion resistance ensures the fuel assemblies' operability to high burnup.

In the new generation reactors, it is assumed that conditions will cause higher stresses in the shells and more intense oxidation processes. In this regard, it is relevant to search for alternative alloys not only for the casings of fuel elements, but also for structural elements of a fuel assembly, such as guide channels, a central pipe, and corners of a rigid frame capable of providing the required fuel resource.

Recently, a multicomponent alloy E635 has been widely used as a material for fuel assemblies of the water-moderated reactor with a capacity of 1000 MW.

http://dx.doi.org/10.18720/MPM.4612020_9

During the transport and technological operations such as fuel movement, loading/unloading of fuel, situations may arise that are accompanied by dynamic influences. To obtain reliable estimates of numerical modeling, it is necessary to use deformation models and strength criteria corresponding to the problem being solved. In dynamics problems, it is important to take into account the strain rate influence on the material characteristics. Extensive experimental research is required to build mathematical models describing this effect.

Despite the widespread use of zirconium alloys in nuclear power engineering, as well as the importance of studying the dynamic properties of alloys based on zirconium, there are very little data on this. Investigations of the mechanical characteristics of the metal alloy E110 were carried out in [1]. In this study, the behavior of a zirconium alloy was studied under shock-wave loading conditions. The authors determined the spall strength at strain rates of 10^5-10^6 s^{-1} using laser interferometers VISAR and POV. At shock compression pressures of above 10.6 GPa it was obtained a three-wave structure of the compression pulse. According to the authors, this effect is associated with polymorphic transformations α-ω. In [2] the dynamic characteristics of the MA-15-Ti magnesium alloy were determined using the Kolsky method. Zirconium is a structure modifier in this alloy and it significantly improves physical and mechanical properties. There are few studies [3-7], which are devoted to the study of the dynamic mechanical properties and microstructural features of deformation in the adiabatic shear bands of amorphous zirconium-based alloys at strain rates about 10^3 s^{-1}. For the investigated alloys an increase in the strength characteristics with increasing strain rate is noted, microstructural features of deformation are revealed and the mechanisms of formation of adiabatic shear bands are studied. In [8-13] the dynamic properties of ceramics based on zirconium are investigated using the Kolsky method and its modifications. Dynamic diagrams of deformation under a uniaxial stress state, as well as strength and deformation properties under uniaxial strain, were obtained.

The present work is devoted to the determination of the strain rate and temperature dependences of the deformation curves and ultimate plasticity characteristics of E110 and E635 zirconium alloys.

2. Test specimens

Specimens of two zirconium alloys E110 and E635 were subjected to quasistatic and dynamic tests. The chemical composition of these alloys is given in Table 1.

Table 1. The chemical composition of tested alloys

Denotation	Mass content, %					
	Zr	Nb	Sn	Fe	O	impurities
E110	Base	0.9-1.1	-	0.05	0.1	0.18
E635	Base	0.9-1.1	1.1-1.5	0.3-0.5	0.1	0.15

The compression test specimens were in the form of cylinders with dimensions Ø = 16 mm L_0 = 8 mm for static tests and Ø = 10 mm L_0 = 5 mm for dynamic tests. For tensile tests, samples with threaded heads had the dimensions of the working part: Ø = 5 mm, L_0 = 15 mm for static tests and Ø = 5 mm, L_0 = 10 mm for dynamic tests.

3. Test methods

Static compression and tensile tests of the specimens at temperatures of + 20ºC and + 350ºC were carried out on a ZwickRoell Kappa 50 DS experimental setup with a maximum loading force of ±600 kN. The measuring equipment included a class 1 force sensor in accordance with ISO 7500-1 and a high-precision displacement meter built into the movable beam of the

machine, with an accuracy of positioning of the beam in a predetermined position of not more than ±2 μm. To obtain the elastic modulus E of the materials, we used a high-precision high-temperature extensometer RMA-12 / V7-1 (resolution 0.1 μm) installed on the working part of the sample and allowing to determine the elastic modulus at normal and elevated temperatures. The testing machine is equipped with a MAYTEC-HT 080/1 heating device.

Compression and tensile tests in the dynamic range of strain rates (5 10^2-5 10^3 s^{-1}) at temperatures +20ºC, +200ºC, and +350ºC were carried out using the Kolsky (or Split Hopkinson Pressure Bar) method [14] and its modifications [15-17]. The following formulas can be used to calculate stress, strain, and strain rate in a specimen based on recorded pulses in the measuring bars:

$$\sigma_s(t) = \frac{EA}{2A_s^0}\varepsilon_1(t), \quad (1)$$

$$\varepsilon_s(t) = \frac{C}{L_0}\int_0^t \varepsilon_2(\theta)d\theta, \quad (2)$$

$$\dot{\varepsilon_s}(t) = \frac{C}{L_0}\cdot\varepsilon_2(t). \quad (3)$$

Here E – elastic modulus of the measuring bar, A – measuring bar's cross-section area, C – sound speed in the measuring bar, L_0 and A_s^0 – initial length and initial cross-section area of the specimen.

Instead of the $\varepsilon_1(t)$ and $\varepsilon_2(t)$, one of three expressions can be substituted, respectively:

– for stress calculation:

$$\varepsilon_1(t) = \begin{cases} \varepsilon^I(t) + \varepsilon^R(t) + \varepsilon^T(t) \\ 2\cdot\left(\varepsilon^I(t) + \varepsilon^R(t)\right) \\ 2\cdot\varepsilon^T(t) \end{cases} \quad (3)$$

– for strain calculation:

$$\varepsilon_2(t) = \begin{cases} \varepsilon^I(t) - \varepsilon^R(t) - \varepsilon^T(t) \\ 2\cdot\left(\varepsilon^I(t) - \varepsilon^T(t)\right) \\ -2\cdot\varepsilon^R(t) \end{cases} \quad (4)$$

Further, from the obtained parametric dependences $\sigma_s(t)$, $\varepsilon_s(t)$ and $\dot{\varepsilon}_s(t)$ time is excluded, and a deformation diagram $\sigma_s(\varepsilon_s)$ of a specimen with a known dependence $\dot{\varepsilon}_s(\varepsilon_s)$ is constructed. During the test, using a strain gauge on measuring bars, a loading stress (strain) impulse is recorded. The shape, amplitude, and duration of this impulse are set by choosing the length, material, and velocity of the striker which is accelerated in the barrel of the gas gun. In addition, stress (strain) pulses reflected from the specimen and transmitted through it are recorded, which are the "responses" of the material to the applied load and allow constructing a dynamic diagram of the test specimen.

An experimental setup that implements the SHPB method includes a pneumatic loading device (gas gun with a caliber of 20 mm) with a control system, a complex of measuring and recording equipment, and replaceable sets of bars made of steel or aluminum alloy with a diameter of 20 mm for testing under various conditions. In the present investigation bars made of high-strength steel with a yield strength of about 2000 MPa are used. The bars are fixed and centered in textolite plain bearings, which allow adjustment of their relative position with the help of adjusting elements to ensure alignment of the bars with each other and with the striker. The strain is measured using small-base strain gauges glued to the lateral surface of the bars at a considerable distance from the specimen. Moreover, to compensate for bending vibrations in the bars and increase the amplitude of the useful signal in the working sections, 4 strain gauges connected in series are glued. To study the behavior of materials at elevated temperatures, a miniature tube-type furnace is used. It warms the ends of the measuring bars with a sample located between them. An XC thermocouple welded to the side

surface of the sample was used to control the temperature of the specimen. At test temperatures up to +350ºC any correction of the formulas and the method of processing experimental information was not performed, since at such temperatures, there are no noticeable changes in the elastic characteristics of the material of the bars (elastic wave velocity and elastic modulus).

4. Test results

The deformation diagrams at static compression and tension of the E110 and E635 alloys were constructed at temperatures T = 20ºC and 350ºC. Three samples were tested at each temperature, and the results were averaged.

Dynamic tests at high strain rate tension were carried out using the Nicholas scheme [16]. Four conditions were implemented in terms of strain rate: 1000, 1500, 2000, and 2800 s^{-1} as well as three conditions in terms of temperature: +20, +200, and + 350ºC. In each loading condition, five specimens were tested to determine the scatter characteristics of the experimental data.

The compression schemes were used to obtain strain curves. The tensile schemes were used to determine the ultimate fracture characteristics.

Figure 1 illustrates the effect of the strain rate on the strain curves of the E110 alloy. Dynamic curves have larger initial yield strength and the angle of the plastic part of the curve. In the strain rate range from 850 to 2400 s^{-1}, the effect of strain rate hardening is weakly expressed.

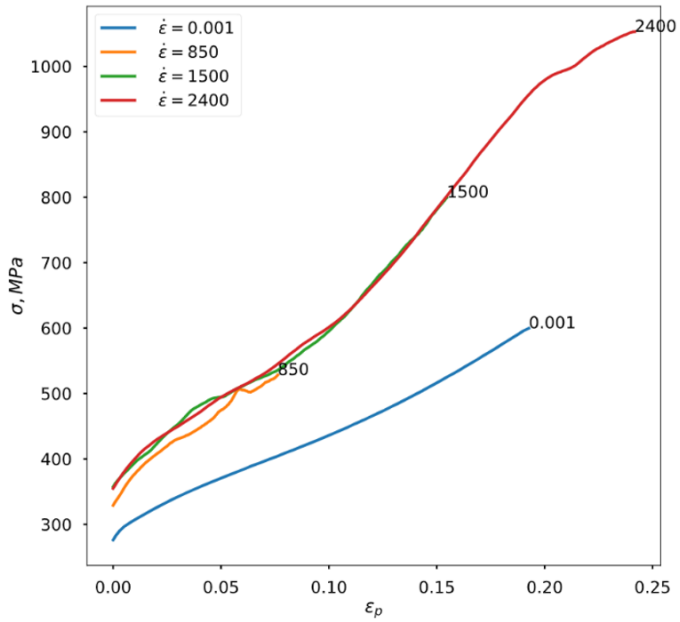

Fig. 1. Strain rate influence on strain curves. E110 alloy

The left side of Fig. 2 illustrates the effect of temperature on the strain curves of E110 alloy. Dashed lines are static curves. The solid lines are the dynamic curves, obtained at strain rate ~1500 s^{-1}. The corresponding temperatures in Celsius degree are shown next to the each line. The right part of Fig. 2 shows slices of curves at different plastic strain levels (the corresponding plastic strain values are shown next to the each line). Dashed lines are static curves. The solid lines are the dynamic curves. If we analyze the results, it turns out that in the static region the influence of temperature is more pronounced. This can be seen by the slope of the curves on the right part of Fig. 2.

Figure 3 shows the deformation curves of the E635 alloy at different strain rates. It can be noted that this material has a higher resistance to deformation than the E110 alloy.

Figure 4 illustrates the effect of temperature on E635. The same effect is observed as in the case of alloy E110.

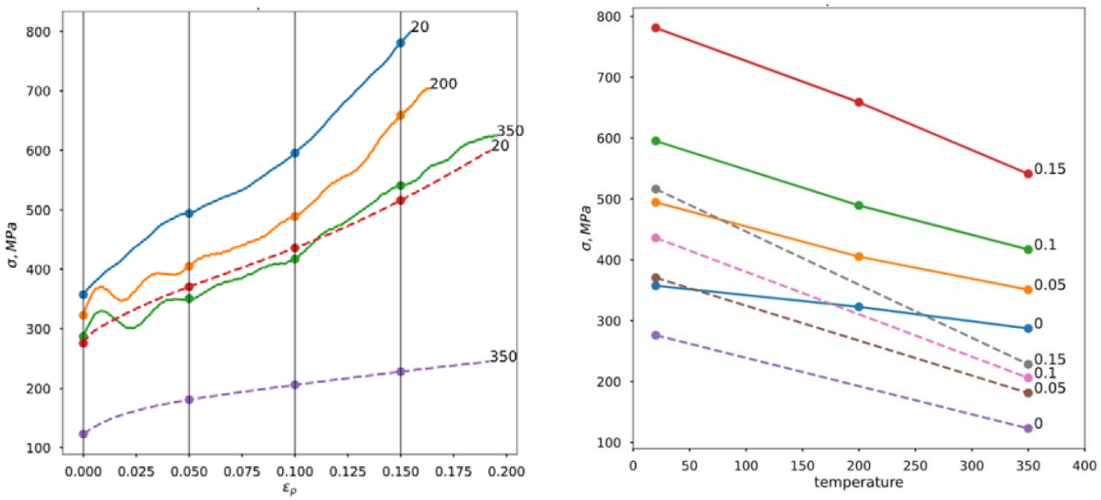

Fig. 2. Temperature influence on strain curves. E110 alloy

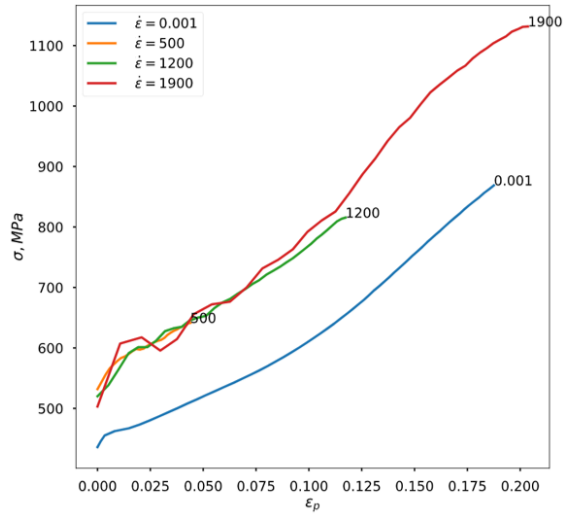

Fig. 3. Strain rate influence on strain curves. E635 alloy

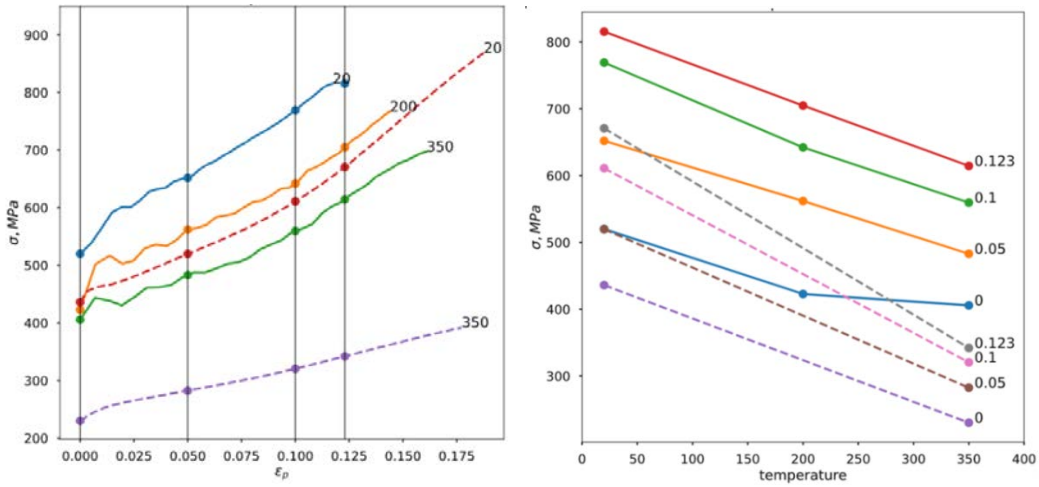

Fig. 4. Temperature influence on strain curves. E635 alloy

Based on the shape of the specimens fractured in tension the ultimate plastic strains were determined using the formula:

$$\varepsilon_p^f = ln\frac{1}{1-\frac{D_0^2-D^2}{D_0^2}}. \quad (5)$$

Here D_0 – initial diameter of the specimen's cross section, D – diameter of the fractured specimen's cross-section in the neck.

The obtained data will be illustrated in the section «Model identification».

5. Model identification

To use in the numerical simulation, the obtained data must be turned into a mathematical model. So, the experimental surfaces were approximated by analytical functions.

The Johnson-Cook model is widely used to describe the dynamic behavior of visco-plastic materials. The mathematical formulation for the dependence of the radius of the yield surface on the strain, strain rate, and the temperature is formulated as follows [18,19]:

$$\sigma = \left(A + B \cdot \varepsilon_p^n\right)\left(1 + C \cdot ln\dot{\varepsilon}_p^*\right)(1 - T^{*m}). \quad (6)$$

Here $T^* = \frac{T-T_0}{T_m-T_0}$, ε_p – equivalent plastic strain, $\dot{\varepsilon}_p^* = \dot{\varepsilon}_p/\dot{\varepsilon}_0$ – dimensionless plastic strain rate, $\dot{\varepsilon}_0$ = 1.0 s^{-1}, T_0 and T_m – room (or reference) temperature and melting temperature respectively. Five material constants are determined empirically: *A, B, n, C* и *m*.

In addition to the classical, linear in the logarithm of strain rate multiplier

$$1 + C \cdot \ln(\dot{\varepsilon}^*), \quad (7)$$

other options exist to take into account the influence of the strain rate on the flow stress:

- model of Huh-Kang [20]:

$$1 + C \cdot \ln(\dot{\varepsilon}^*) + C_2 \cdot \ln(\dot{\varepsilon}^*)^2, \quad (8)$$

- model of Cowper-Symonds [21]:

$$1 + \left(\frac{\dot{\varepsilon}^*}{C}\right)^{\frac{1}{p}}, \quad (9)$$

- model of Allen-Rule-Jones [22]:

$$(\dot{\varepsilon}^*)^C. \quad (10)$$

Approximation independent material characteristics for E110 and E635 alloys are shown in Table 2.

Table 2. E110 and E635 properties

Property	Value	Dimension
Density, ρ	6600	kg/m^3
Young's modulus, E	95	GPa
Poisson's ratio, ν	0.34	
The melting temperature, T_m	2106	K
T_0	293	K
Specific heat, c_p	0.24	kJ/kg/K

The disadvantage of the model is that the various effects are independent of each other. Thus, due to the multiplicative formulation, the temperature softening is the same for statics and dynamics, which does not allow us to describe the effect obtained earlier.

You can either focus on static data and well describe the effect of temperature in statics. In this case, the dynamic curves at different temperatures are poorly described (left side of Fig. 5). On the other hand, we can approximate dynamic curves well and get a poor description of static temperature softening (right side of Fig. 5).

In Figure 5 dotted lines correspond to experimental curves, solid ones – to the mathematical model. Blue color indicates data at room temperature, orange – at temperature 200ºC, and red – at temperature 350ºC. Parameters of the mathematical model for static and dynamic temperature softening cases are given in Tables 3 and 4.

Table 3. Johnson-Cook parameters. E110, focus on static temperature softening

A	324	MPa
B	3684	MPa
n	1.324	
C	0.032	
m	0.36	

Table 4. Johnson-Cook parameters. E110, focus on dynamic temperature softening

A	325.4	MPa
B	3756	MPa
n	1.34	
C	0.032	
m	0.73	

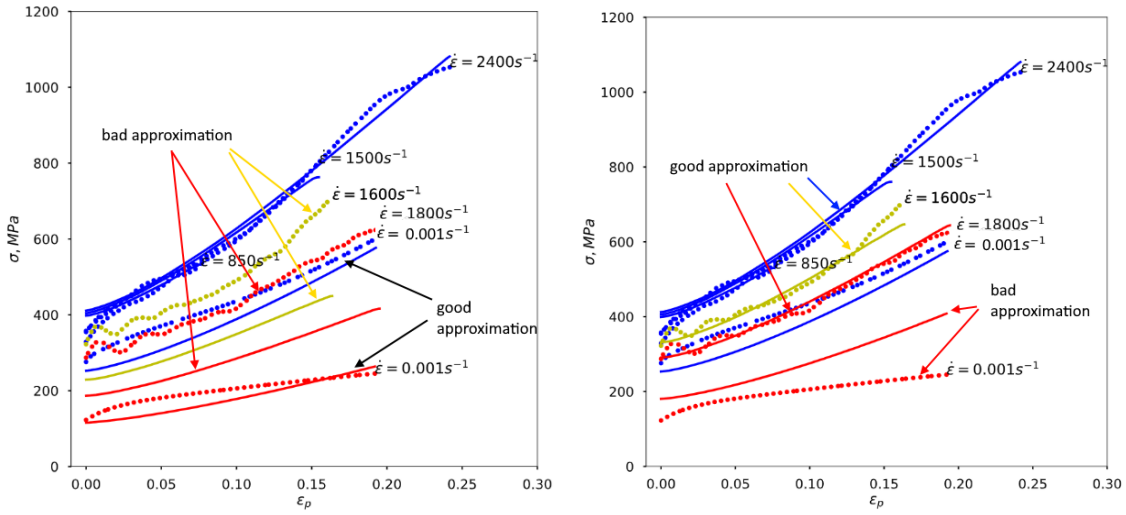

Fig. 5. E110 data approximation by the Johnson-Cook equation

In addition, the modified Johnson-Cook model was considered [6]:

$$\sigma = \sigma_A + B \cdot e^{-(\beta_0 - \beta_1 ln\dot{\varepsilon})T} + A \cdot \varepsilon^n \cdot e^{-(\alpha_0 - \alpha_1 ln\dot{\varepsilon})T}. \quad (11)$$

Here σ_A, B, β_0, β_1, A, n, α_0, α_1 – model's parameters.

This model has more parameters but allows describing more complex effects. It can be seen from Fig. 6 that this model allowed us to approximate the experimental data with sufficient accuracy. Modified Johnson-Cook parameters for E110 and E635 alloys are shown in Table 5.

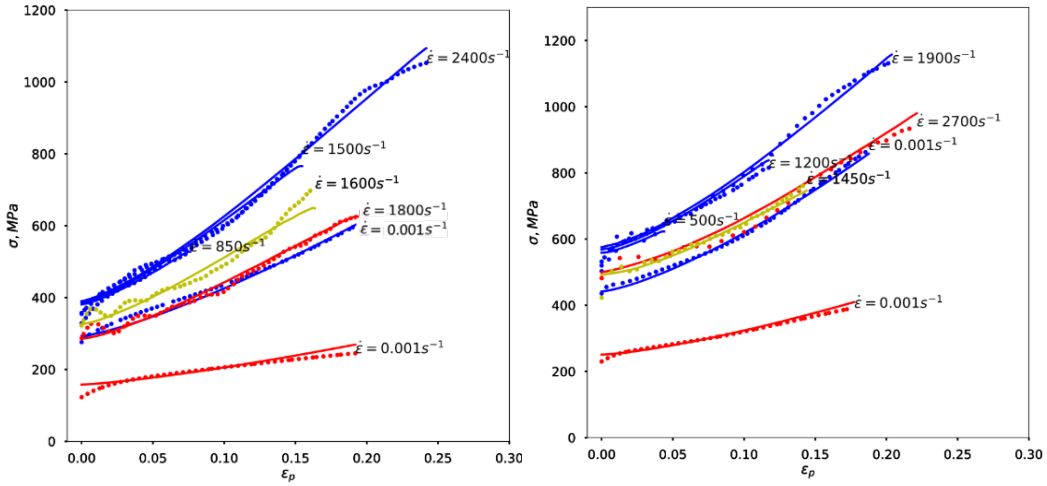

Fig. 6. Data approximation by the modified Johnson-Cook equation for E110 (left) and E635 (right)

Table 5. Modified Johnson-Cook parameters

	E110	E635	
σ_A	0	0	MPa
B	507	730	MPa
β_0	0.0014	0.0013	
$\beta 1$	$6.4 \cdot 10^{-5}$	$5.9 \cdot 10^{-5}$	
A	6512	8956	MPa
n	1.3	1.36	
α_0	0.0022	0.0022	
$\alpha 1$	0.00013	$6.43 \cdot 10^{-5}$	

The obtained strain rate and temperature dependence of the ultimate plastic strain were approximated by the model:

$$\varepsilon_p^f = D_1 \cdot (1 + \dot{\varepsilon})^{D_4} \cdot \left(1 + D_5 \cdot \frac{T - T_0}{T_m - T_0}\right). \quad (12)$$

Parameters of approximation are given in Table 6.

Table 6. The ultimate plastic strain approximation parameters

	E110	E635
D_1	0.17	0.22
D_4	0.181	0.1
D_5	5.83	3

Figure 7 illustrates the dependence of the ultimate plastic strain on strain rate and temperature. Markers correspond to experimental data obtained at different temperatures. The solid line corresponds to the mathematical model. It can be noted that the ultimate strain increases slightly with increasing strain rate and significantly increases with temperature rise.

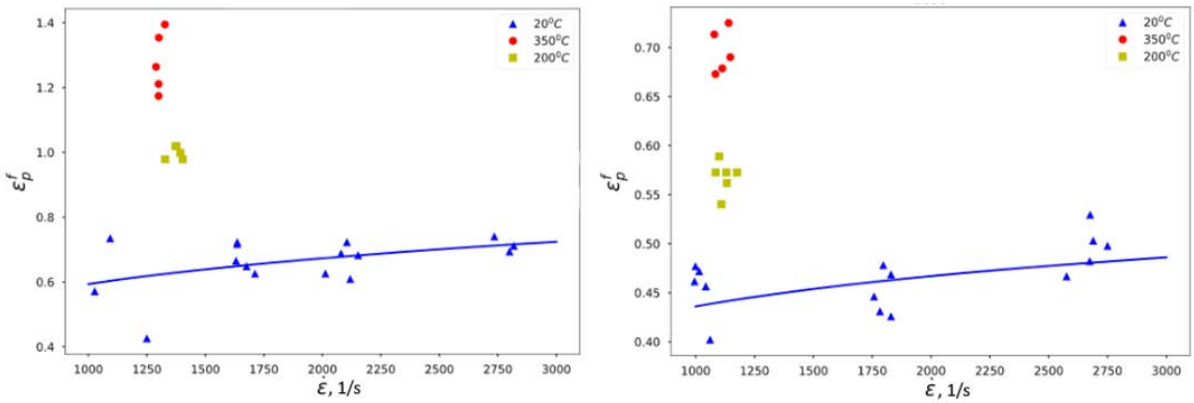

Fig. 7. Ultimate plastic strain for E110 (left) and E635 (right)

Figure 8 illustrates the approximation of the temperature dependences of the fracture strain for the studied alloys. It can be noted that the E635 alloy is fractured at lower values of plastic strain. The temperature has a greater effect on the ultimate characteristics of the E110 alloy.

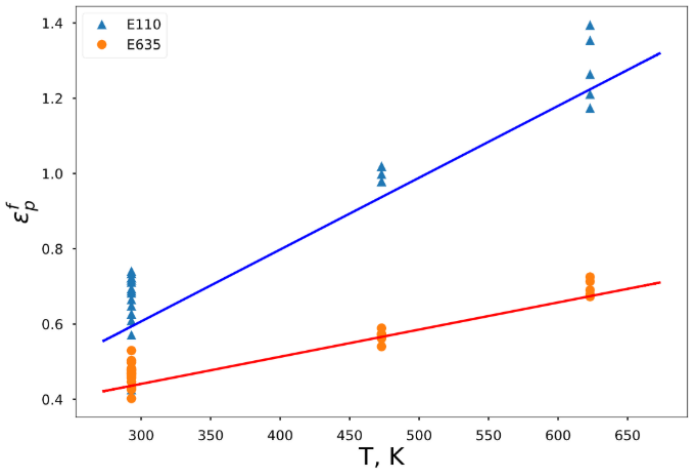

Fig. 8. Temperature dependence of ultimate plastic strain for E110 (left) and E635 (right) and its approximations

6. Conclusions

As a result of the investigation of deformation of alloys E110 and E635 under compression and tension in a wide range of strain rates and temperatures from 20ºC up to 350ºC, mechanical characteristics are obtained in the form of deformation diagrams. It is noted that the mechanical behavior of the investigated alloys is sensitive to the strain rate and temperature. Obtained data is approximated by the modified Johnson-Cook model reasonably well. E635 alloy has a higher resistance to deformation than the E110 alloy but is fractured at lower values of plastic strain. The temperature has a greater effect on the ultimate characteristics of the E110 alloy than on the E635 alloy. As a result of the study, the mathematical models of the deformation and strength criteria are constructed which can be used in the development of digital copies of nuclear engineering designs.

Acknowledgements. *Experimental investigations were financially supported by the Federal Targeted Program for Research and Development in Priority Areas of Development of the Russian Scientific and Technological Complex for 2014-2020 under the contract No. 075-15-2019-1702 (unique identifier RFMEFI60519X0183). Theoretical studies were carried out*

within the Grant of the President of the Russian Federation for young scientists (MD-1221.2019.8).

References

[1] Kazakov DN, Kozelkov OE, Mayorova AS, Malyugina SN, Mokrushin SS, Pavlenko AV. Dynamic behavior of zirconium alloy E110 under submicrosecond shock-wave loading. *EPJ Web of Conferences*. 2015;94: 02021.

[2] Bragov AM, Konstantinov AY, Lomunov AK, Petrovtsev AV. The dynamic properties of zirconium-containing magnesium alloy MA14-T1. *Materials Physics and Mechanics*. 2016;28(1/2): 101-105.

[3] Zou DL, He LF, Xiao DW. Evolution of adiabatic shear bands in zirconium alloy under dynamic deformation. In: *3rd International Conference on Material, Mechanical and Manufacturing Engineering (IC3ME 2015)*. 2015. p.2031-2034.

[4] Koteneva MV, Nikulin SA, Rozhnov AB, Rogachev SO. Structure and mechanical properties of oxide films on zirconium alloys upon oxidation under different conditions. *Prot. Met. Phys. Chem. Surf.* 2014;50: 64-68.

[5] Zou DL, Luan BF, Liu Q. Microstructural evolution of zirconium alloy under dynamic compression at strain rate of 1000 s−1. *Transactions of Nonferrous Metals Society of China.* 2012;22(10): 2402-2408.

[6] Skripnyak VA, Skripnyak EG. Mechanical Behavior of Nanostructured and Ultrafine-Grained Metal Alloy under Intensive Dynamic Loading. In: Vakhrushev A. (Ed.) *Nanomechanics*. Available drom: 10.5772/intechopen.68291.

[7] Guo YK, Zou DL, Shuai MB, Xiao DW. Dynamic deformation evolution of zirconium alloy impacted by split Hopkinson pressure bar. In: *Advanced Materials and Energy Sustainability*. 2017. p.310-314.

[8] Bragov AM, Kramarev LN, Lomunov AK, Mineev VN, Akopov FA, Cherny`shov GP, Vlasov AS, Lukin SS. High-rate deformation and destruction of zirconia ceramics. *Problems of strength and plasticity.* 2000;62: 144-158. (In Russian)

[9] Bragov AM, Lomunov AK, Mineev VN, Akopov FA, Chernyshov GP. Dynamic properties of zirconium dioxide refractories. *Journal of Applied Mechanics and Technical Physics*. 2001;42(3): 523-528.

[10] Bragov AM, Lomunov AK, Mineev VN, Kruszka L. High strain-rate deformation and fracture of the dioxide-zirconium ceramics. In: Nowacki WK, Klepaczko JR. (Eds.) *New Experimental Methods in Material Dynamics and Impact. Trends in Mechanics of Materials.*, eds. Warsaw; 2001. p.349-356.

[11] Akopov F, Bragov AM, Demenko P, Kruszka L, Lomunov AK, Mineev V, Sergeichev IV. Static and dynamic response of ceramics and zirconium alumina concrete materials. *J.Phys. IV. France.* 2003;110: 231-236.

[12] Bragov A, Kruszka L, Lomunov A, Konstantinov A, Lamzin D, Filippov A. High-speed deformation and fracture of the dioxide-zirconium ceramics and zirconium alumina concrete. *The European Physical Journal. Web of Conferences.* 2012;26: 01055.

[13] Skripnyak VA, Bragov AM, Skripnyak VV, Lomunov AK, Skripnyak EG, Vaganova IK. Fracture mechanisms of zirconium diboride ultra-high temperature ceramics under pulse loading. *AIP Conference Proceedings.* 2017;1793(1): 100003.

[14] Kolsky H. An investigation of the mechanical properties of material at very high rates of loading. *Proc. Phys. Soc. (London).* 1949;62B: 676-700.

[15] Nicholas T, Rajendran AM. Material characterization at high strain-rates. In: Zukas JA. (Ed.) *High Velocity Impact Dynamics*. NY: Wiley; 1990. p.127-296.

[16] Nicholas T. Tensile testing of materials at high rates of strain. *Exp.Mech*. 1981;21(5): 177-195.

[17] Bragov AM, Lomunov AK. Methodological aspects of studying dynamic material properties using the Kolsky method. *Int. J. Impact. Engng.* 1995;16(2): 321-330.
[18] Johnson GR, Cook WH. A constitutive model and data for metals subjected to large strains, high strain rates and high temperatures. In: *Proceedings of the Seventh International Symposium on Ballistic*. The Hague, The Netherlands;1983. p.541-547.
[19] *LS-DYNA Keyword User's Manual - Volume II, Material Models.* Available from: https://www.dynamore.se/en/. [Accessed 21th December 2020].
[20] Huh H, Kang WJ. Crash-Worthiness Assessment of Thin-Walled Structures with the High-Strength Steel Sheet. *International Journal of Vehicle Design*. 2002;30(1/2): 1-21.
[21] Cowper GR, Symond PS. *Strain Hardening and Strain Rate Effects in the Impact Loading of Cantilever Beams.* Brown University: Applied Mathematics Report; 1958.
[22] Allen DJ, Rule WK, Jones SE. Optimizing Material Strength Constants Numerically Extracted from Taylor Impact Data. *Experimental Mechanics*. 1997;37(3): 333-338.